

Article

Investigation of the Mechanical Properties of Additively Manufactured Metal Parts with Different Relative Densities

Itthidet Thawon , Thongchai Fongsamootr, Yuttana Mona and Pana Suttakul * Department of Mechanical Engineering, Faculty of Engineering, Chiang Mai University,
Chiang Mai 50200, Thailand

* Correspondence: pana.s@cmu.ac.th

Abstract: Currently, metal additive manufacturing (MAM) has been receiving more attention in many sectors for its production of metal parts because MAM effortlessly enables the fabrication of complex metal parts and provides faster and more sustainable manufacturing than conventional processes. Recently, a MAM-using bound metal deposition (BMD) has been proposed as a user-friendly manufacturing method that can provide low-volume production, economical metal parts, and operation safety. Since the BMD technique is new, information on the mechanical properties of MAM parts using this technique has not been sufficiently provided. This paper aims to study the mechanical properties of MAM parts manufactured by the BMD technique, examining the elastic modulus, yield strength, ultimate strength, and fatigue behavior of the parts with different relative densities. The MAM parts made from 316L and 17-4PH stainless steel were investigated using tensile and fatigue tests. Some mechanical properties of the infill parts in this study were validated with formulas from the literature. The weight efficiency is used as an index to assess the efficiency of the infill parts with different densities by examining the relationship between the mechanical properties and the weight of the MAM parts. The experimental results and a discussion of the weight efficiency assessment are presented as a novel information report on MAM products fabricated by BMD technology.

Keywords: metal additive manufacturing; bound metal deposition; 316L stainless steel; 17-4PH stainless steel; tensile test; fatigue test; infill density



Citation: Thawon, I.; Fongsamootr, T.; Mona, Y.; Suttakul, P. Investigation of the Mechanical Properties of Additively Manufactured Metal Parts with Different Relative Densities. *Appl. Sci.* **2022**, *12*, 9915. <https://doi.org/10.3390/app12199915>

Academic Editors: Junwon Seo and Jong Wan Hu

Received: 30 June 2022

Accepted: 5 August 2022

Published: 1 October 2022

Publisher's Note: MDPI stays neutral with regard to jurisdictional claims in published maps and institutional affiliations.



Copyright: © 2022 by the authors. Licensee MDPI, Basel, Switzerland. This article is an open access article distributed under the terms and conditions of the Creative Commons Attribution (CC BY) license (<https://creativecommons.org/licenses/by/4.0/>).

1. Introduction

Materials' processing technology has been continuously developed to improve production efficiency and quality. Computer-aided manufacturing (CAM), one of the most interesting technologies available, offers convenience and cost reduction for manufacturing by using a computer-aided design (CAD) [1]. In the past, most CAM technologies used only subtractive manufacturing that lost the cut material, such as computer numerical control (CNC), waterjet, and laser cutting. Nowadays, additive manufacturing (AM) or 3D printing is widely used for fabricating complex parts as an up-to-date CAM [2]. AM technologies can help to reduce material costs and manufacturing time by additively fabricating layer by layer to form the shape as designed by the CAD file. Additionally, these technologies can produce parts with desired material behavior, such as optimized shape and density for specific material properties. With these advantages, AM technologies are widely used in many industries, such as medical, automotive, and aerospace [3–7]. Particularly in aerospace industry, a lightweight design of the components for spacecraft was presented by [4,5]. The material behavior of the components manufactured by AM was studied by adjusting the print parameters. The development and implementation of AM in the aerospace industry were comprehensively reviewed by [6,7], in which the primary applications and associated commercial and technical benefits were summarized.

An AM part can be designed by adjusting its print parameters, such as the number of layers, layer height, wall thickness, infill density, infill pattern, pattern orientation, etc.

Many researchers have studied the impacts of print parameters, resulting in the mechanical properties of AM parts using the tensile test [8–13]. For example, Hsueh et al. [9] studied the effect of infill density on the mechanical behavior of polylactic acid specimens fabricated by means of fused deposition-molding technology. The study showed that the Young's modulus is significantly impacted by infill density. In a study by [10], the effect of infill density with a triangular infill pattern on mechanical properties of seven different plastic materials was investigated using the tensile test. The results showed that the yield strength and Young's modulus are directly affected by infill density. As the infill density increased, the tensile yield strength and Young's modulus increased. Their study also showed that, for some materials, the failure mode also depends on infill density. The effect of layer parameters on the mechanical properties of plastic AM parts made from acrylonitrile butadiene styrene was experimentally investigated by [12]. Specimens were printed with two different print parameters, i.e., print directions and the number of layers, while the layer height was set as a constant value for all layers. The results show that the print direction impacts the strength of specimens in every number of layers considered. The strength and Young's modulus became constant at twelve layers or more. The effects of print parameters, e.g., nozzle diameter, on metal AM parts made from 316L stainless steel were investigated by [13]. It was found that a smaller nozzle diameter gives more geometrical accuracy, but that the mechanical performance decreases. The influence of print parameters on the flexural properties of metal AM parts was also studied by [14], in which build orientation effects were investigated.

In recent years, metal additive manufacturing (MAM) has received more attention in many sectors for producing metal parts. A well-known MAM technique is powder bed fusion (PBF), which spreads powder to form a metal part fused selectively by a high-energy beam. Since PBF needs strict safety regulations and is expensive, extrusion-based MAM methods are considered an alternative for manufacturing more accessible and safer metal parts without dust and lasers. Recently, bound metal deposition (BMD), a new extrusion-based MAM technology based on material extrusion processes, in which material is selectively dispensed through a nozzle, has been offered by Desktop Metal. This technique can enable low-volume production and economical metal parts. Various materials can be fabricated using the BMD, such as stainless steel, copper, and titanium. The raw material is in the form of a rod comprising a mix of metal powder, wax, and binder. The metal and ceramic rods contained in extruders are fed and fused to form a metal part and ceramic support media, respectively, in the print process. Next, the binder is dissolved in the debinding process and is then densified in the sintering process. After metal particles fuse as a 3D object, the ceramic interface can be removed to obtain the final part. The AM parts fabricated using the BMD can be divided into three portions, i.e., infill structure, side wall, and top/bottom wall, as shown in Figure 1.

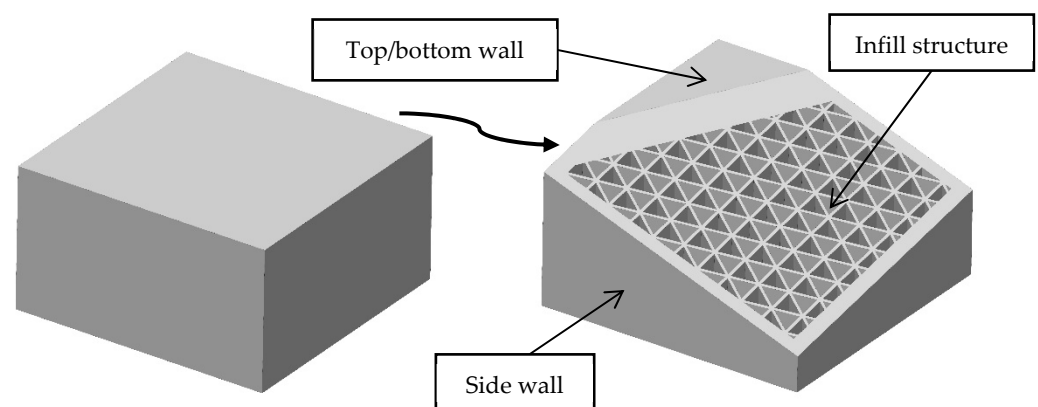


Figure 1. The components of an AM part with the BMD technique.

Most AM technologies can print a part with an infill density to reduce the consumption of raw materials and make the part with a lightweight feature. An AM part with an infill pattern inside can be treated as a lattice structure consisting of a number of unit cells. Lattice structures have been widely used as infill structures of AM parts because their mechanical properties can be efficiently designed by adjusting their unit cells. The mechanical properties of lattice structures with various patterns have been studied by many researchers [15–25]. For example, isotropic in-plane elastic properties of lattice structures with triangular unit cells were confirmed by an analytical study by [15] and an experimental study by [16]. Methods to determine the effective properties of lattice structures have also been investigated; in a study by [17], the effective in-plane properties were derived by an analytical method. Theerakittayakorn et al. [18] proposed the exact forms of effective elastic properties of lattice structures with different patterns using exact curve fitting. In the same lattice structures studied, Sam et al. [19] presented the derivation of closed-form effective elastic properties of the lattice structures using a generic symbolic finite element program. Effective in-plane material properties of 2D hexagonal lattices with and without considering the shear deformation of their struts were presented by [22]. The numerical and experimental investigations of in-plane and bending material behaviors of 2D lattice structures with various unit-cell patterns were proposed by [24,25], respectively. In AM technologies using the BMD, a lattice structure with a triangular pattern was generally used as the infill pattern of AM parts. The mechanical properties of the AM parts can be optimized by modifying some significant print parameters related to the infill structure to achieve a light weight and sufficient strength for their applications, e.g., layer, density, and orientation.

Print parameters influencing the mechanical properties of MAM parts fabricated using the BMD include infill density, side wall thickness, top/bottom wall thickness, and pattern orientations. Among the print parameters, infill density is directly related to the raw material used and the performance of AM parts, as well as time and cost in the manufacturing process. Consequently, the relationship between mechanical properties and infill density plays a significant role in assessing the specific performance of different infill parts. To date, few studies have reported the mechanical properties of metal parts fabricated using BMD [26–28]; in addition, no works emphasizing the influence of infill density on the mechanical properties are yet available. Bjørheim and Lopez [26] experimentally investigated the mechanical properties of additively manufactured specimens of 17-4PH processed by BMD using a tensile test. Three printing orientations with raster directions were investigated to observe the changes in the mechanical properties of the specimens. They found that the specimens printed on a plane with a raster horizontal direction show the highest ultimate strength and elongation and behave as ductile materials. In contrast, the specimens printed in raster vertical directions almost act as brittle materials. The results show that the specimens with different print orientations yield anisotropic behavior. This behavior is also indicated in the prediction of fatigue behavior estimated from the tensile results. The mechanical properties of 316L stainless steel parts manufactured using BMD were studied by [27]. Print parameters, which varied in their study, included build orientation, chamber temperature, and infill pattern. Build orientations consist of horizontal and vertical directions. Chamber temperatures were investigated at room temperature and at 50 °C. The infill patterns include a concentric pattern filled by wall thicknesses and a $\pm 45^\circ$ raster pattern layered by top/bottom thicknesses. They concluded that the specimens built in the horizontal direction have higher ultimate strength than those in the vertical direction. The $\pm 45^\circ$ raster pattern presented a slightly higher ultimate strength rating than the concentric pattern. In addition to the studies on the mechanical properties, Gao et al. [29] reported on the energy efficiency and lifecycle of AM parts using the BMD.

Many metal materials can be used as raw materials in MAM technologies, especially stainless steel. In BMD technology, 17-4PH and 316L are basic print materials for AM parts. 17-4PH stainless steel is characterized by its strength, hardness, and corrosion resistance, making it suitable for various applications, e.g., tooling, molds, and production parts. 316L

stainless steel is a fully austenitic stainless steel, characterized by its corrosion resistance and performance at high and low temperatures. It is often used in chemical processing, saltwater environments, and household or industrial fixtures. Consequently, 17-4PH and 316L are commonly used in many sectors, and their mechanical behavior has been widely investigated [13,14,26–28,30,31]. In reality, materials are usually loaded with a cyclic load, leading to failure due to fatigue. Due to its ductility, 316L stainless steel is often used to carry a cyclic load. The mechanical properties of 316L stainless steel under cyclic loading have been studied by a group of researchers [32–37]. Some of them investigated the fatigue behavior of 316L stainless steel fabricated by MAM technologies. The fatigue behavior of MAM parts made from other materials was also explored [38–42].

Since the BMD is a new and attractive technique for MAM technologies, the mechanical properties of productions fabricated using the BMD have not been studied sufficiently, especially on fatigue performance. This study intends to investigate the mechanical properties of MAM parts, i.e., 316L and 17-4PH stainless steel, fabricated using the BMD technique. The considered mechanical properties of the metal parts are elastic modulus, yield strength, ultimate strength, and fatigue limit. The metal specimens with different infill densities ranging from approximately 50% to 75% of the relative density are investigated. All samples are designed for a tensile test according to the ASTM E8/E8M standard [43]. Some mechanical properties obtained from the tensile test are validated by analytical results from the literature [17,19]. Additionally, according to the ASTM E466 standard [44], the fatigue test is performed to study the fatigue life of the metal parts. The ratio between the weights of each infill specimen and the full-solid counterpart is considered as the weight density of the specimens with different infill densities. The weight efficiency is defined as the relationship between the performance per weight density of an infill specimen and the performance per weight density of a full-solid specimen with the same dimensions. The weight efficiency can be used to assess the efficiency among the infill specimens with different densities.

2. Materials and Methods

2.1. Specimen Preparation

The specimens, made from 316L and 17-4PH stainless steel, were fabricated using the BMD technique using a Studio System Desktop Metal 3D printer. The chemical composition of the specimens is presented in Table 1.

Table 1. Chemical composition of the 316L and 17-4PH stainless steel specimens.

Material	Element ¹ (%)					
	C	Cr	Ni	Mo	Mn	Si
316L	<0.045	16–18	10–14	2–3	<2	<1
17-4PH	C	Cr	Ni	Cu	Mn	Nb + Ta
	<0.07	15.5–17.5	3–5	3–5	<1	0.15–0.45

¹ The data are provided on the official website of Desktop Metal.

Before the manufacturing process, a CAD model of the specimens was created using the SolidWorks program. The CAD file was uploaded on a fabricate web browser of Desktop Metal to set the print parameters, such as layer height, wall thickness, top/bottom thickness, infill density, and orientation. According to the ASTM E8/E8M standard (sheet type), the geometry and dimensions of all specimens with a constant thickness of 3 mm were designed and fabricated.

Because the 3D printer used in this work can only set the infill density to a maximum of 35%, infill densities of 16%, 20%, and 24% were considered. The varying infill densities, in which a triangular infill pattern was used as default, were set via the print parameter setting. The characteristic length of the triangular pattern with infill densities of 16%, 20%, and 24% is 3.0 mm, 2.4 mm, and 2.0 mm, respectively. The cross-sections of all struts in the infill structures are rectangular sections of $0.5 \times 3.0 \text{ mm}^2$. A constant wall thickness of

0.5 mm was set to enclose all side edges of the specimens without top and bottom surfaces. The layer height was set to be a constant of 0.15 mm for all the specimens; consequently, there were 20 layers for each specimen. The print orientation was set to build in a raster horizontal direction, parallel to the build plate, as shown in Figure 2a, to ensure that all samples yield the best performance and ductile behavior [26,27]. The parameter setting of specimens with an equivalent 100% density (the full-solid samples) was the same as those of infill specimens, except for adding the top and bottom layers with a total thickness of 3 mm.

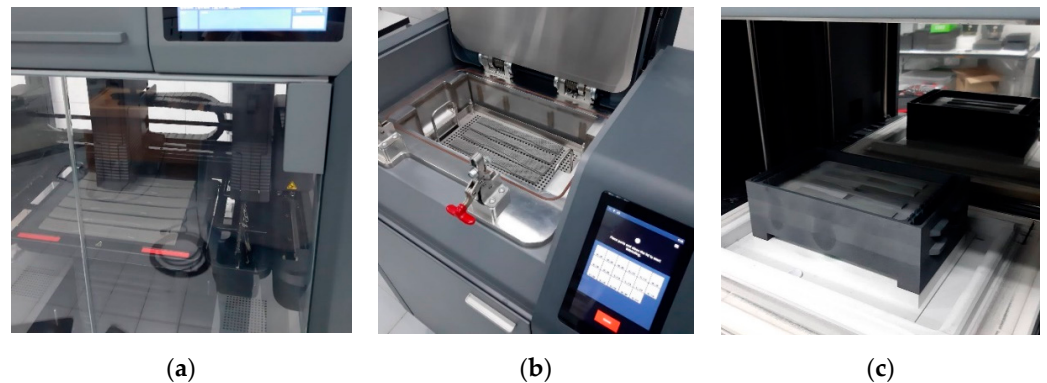


Figure 2. MAM processes using the BMD technique (a) printing, (b) debinding, and (c) sintering.

After the parameter setting, a task was created and then submitted to the printer. The specimens were printed automatically in the printing process. A specimen from the printing process is called a green part, and the dimensions were larger than the size designed. Next, the green parts were placed into a debinding tank, as shown in Figure 2b, to dissolve the binder and create an open-pore channel structure for sintering. A specimen from the debinding process is called a brown part, and these specimens were soft and breakable. The last step was the sintering process, in which the brown parts were placed into the furnace to be densified, as shown in Figure 2c. In this process, the specimens were heated to a temperature close to the melting state. Some remaining binder and wax were removed to provide micro void space for fusing the metal particles. After the sintering process, the finished parts became harder and were shrunk to the designed dimensions, as shown in Figure 3.

The weights of the specimens with different infill densities were measured to compute the relative density of each infill specimen, which is defined by the weight of an infill specimen divided by the weight of the full-solid specimen (see Figure 3). The average relative densities of the specimens are shown in Table 2.

Table 2. The average values of weight and relative density of infill and full-solid specimens.

Material	Infill Density (%)	Weight ¹ (g)	Relative Density ² (%)
316L	16	38.52 (0.07)	50.48
	20	47.21 (0.06)	61.87
	24	55.66 (0.08)	72.94
	Full-solid	76.31 (0.11)	100 (equivalent)
17-4PH	16	39.26 (0.02)	50.68
	20	48.17 (0.03)	62.19
	24	57.01 (0.03)	73.60
	Full-solid	77.46 (0.07)	100 (equivalent)

¹ Standard deviation is depicted in the brackets (SD). ² The infill density is a parameter in the print setting; however, the relative density is a density computed by the actual weight of an infill specimen normalized by that of the full-solid counterpart.

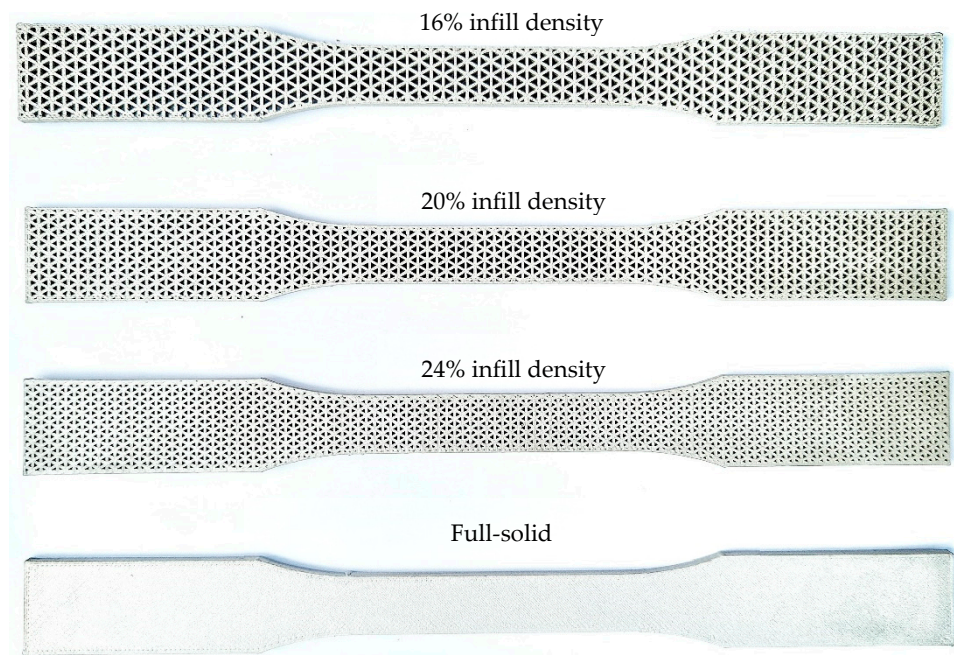


Figure 3. The finished infill and solid specimens.

2.2. Tensile Test

In this study, tensile testing was carried out by an Instron 8802 universal testing machine to obtain the elastic modulus, yield strength, and ultimate strength according to the ASTM E8/E8M standard. The tensile test was performed with displacement control with a 1.0 mm/min speed from the beginning and 5.0 mm/min speed after the yield point. An extensometer was used to measure strain during the elastic region, as shown in Figure 4, and then removed after the yield point. In the plastic region, the strain was measured by crosshead displacement. Six samples were tested for each relative density of 316L and 17-4PH specimens to achieve sufficiently correct data.



Figure 4. Set up of tensile test with an extensometer.

2.3. Fatigue Test

In the fatigue test, the geometry and dimensions of specimens and the testing machine were the same as in the tensile test. The specimens, made from 316L stainless steel, were selected for this test because their ductility behavior is attractive in many applications.

Fifteen samples were tested for each relative density to capture comprehensive data over the stress level range. The load control with a sinusoidal wave according to the ASTM E466 standard was used. The specimens were tested under tension–tension stressing (stress ratio; $R = 0.1$) with a frequency of 30 Hz. A maximum load was defined underneath the ultimate strength of each specimen with different relative densities, while a minimum load level was set related to 10% of the maximum load. The number of cycles at each load level was collected. The maximum stress achieving a fatigue life of 10^6 cycles was considered a fatigue threshold or runout. The specimens were tested with varying stress levels to obtain a trend of fatigue life, presented as S–N diagrams describing the fatigue behavior of the specimens with different relative densities.

2.4. Analytical Method

An inhomogeneous solid in which the inhomogeneities are distributed periodically can be considered as a lattice structure. In artificial lattice structures, such periodic patterns are used to help reduce the amounts of materials used compared to making original solids while retaining the desired properties of the original solids. If a lattice structure consists of a substantial number of unit cells, then the effective properties of the structure can be determined [45].

An infill specimen in this study is constructed by a lattice structure and bounded by side walls. Since the infill pattern of the MAM parts is periodic, the infill specimens with the triangular pattern can be treated as lattice structures with triangular unit cells. Figure 5 shows the lattice structure with triangular unit cells, in which l denotes the characteristic length of the unit cells while $b \times t$ denotes cross-sections of the unit-cell struts. The theoretical relative density of a lattice structure with triangular unit cells can be expressed as [46]

$$\bar{\rho}_{tri} = 2\sqrt{3}\frac{b}{l} \quad (1)$$

where b and t denote the width and thickness, respectively; b is designed to be a constant, l can be varied to adjust the relative density of a lattice structure.

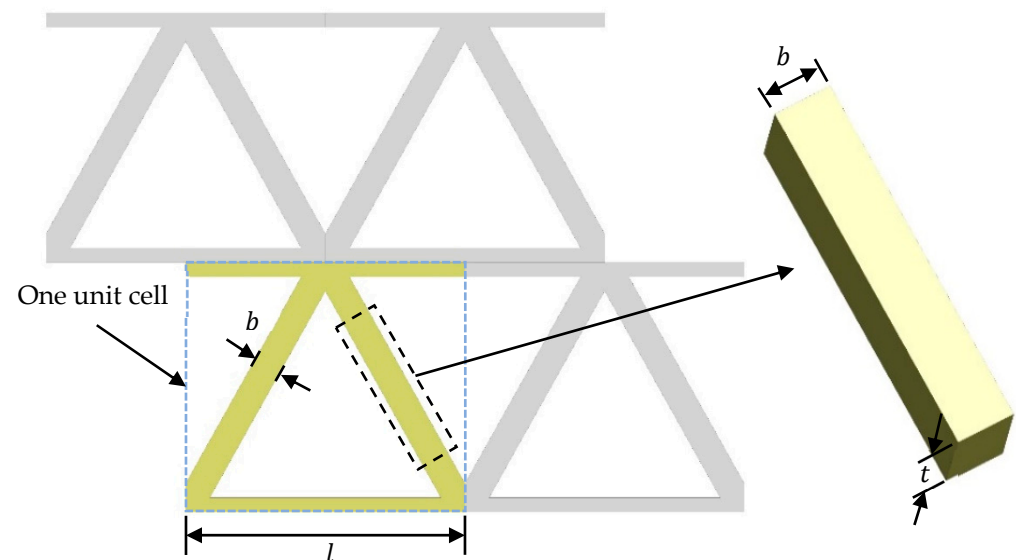


Figure 5. A lattice structure with triangular unit cells.

The elastic properties of the lattice structures with the triangular unit cells can be found in the literature. Analytical forms of the effective elastic modulus E_{tri} and yield strength $\sigma_{y, tri}$ of the lattice structure with the triangular pattern derived by Wang and McDowell [17] can be written as

$$E_{tri} = 0.333\bar{\rho}_{tri}E_s \quad (2)$$

$$\sigma_{y, tri} = 0.5\bar{\rho}_{tri}\sigma_{ys} \tag{3}$$

where E_s and σ_{ys} denote the elastic modulus and yield strength of the base material, respectively. Equations (2) and (3) were constructed with the assumption that the struts were considered as short columns with $b/l \approx 0.1$ to 0.15. For Equation (3), the perfectly plastic deformation was considered for every strut. The effective yield strength was based on the first strut that achieved the yield limit.

Moreover, in a study by Sam et al. [19], a generic symbolic finite element program was used to derive the closed-form effective elastic modulus of lattice structures with triangular unit cells using the strain–energy–based homogenization method. The struts of the lattice structure were modeled as frame structures using Euler’s beams. The effective elastic modulus of the lattice structure with triangular unit cells is written as

$$E_{tri} = \frac{l^2 + b^2}{3l^2 + b^2}\bar{\rho}_{tri}E_s \tag{4}$$

Since the lattice structure with triangular unit cells is bounded by the two side walls, as shown in Figure 6, it is necessary to include the stiffness of the side walls into the overall properties. Rule-of-mixtures models or strength-of-materials models [47] were used to determine the overall elastic modulus $E_{overall}^*$, i.e.,

$$E_{overall}^* = \frac{W_{tri}}{W}E_{tri} + \frac{W_s}{W}E_s \tag{5}$$

where W_{tri} and W_s denote the widths of the lattice structure and the solid wall portion, respectively. In addition, W denotes the overall width of the specimen.

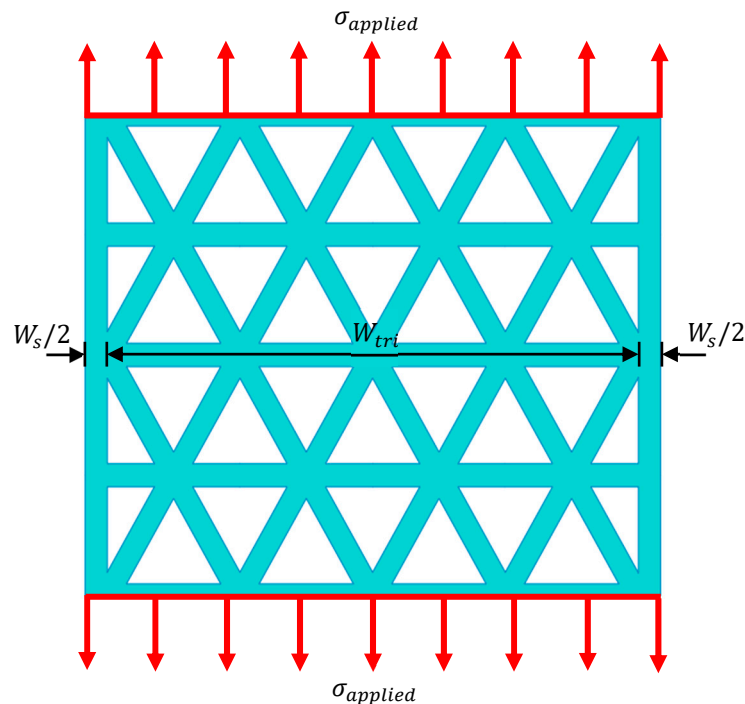


Figure 6. The overall structure of a specimen and its components: solid wall portion (wall side thickness) and triangular lattice portion (interior).

Similarly, the overall yield strength can be derived using the rule-of-mixtures model. The overall yield strength $\sigma_{y,overall}^*$ divided into two conditions, depending on which portion reaches the yield point first, can be expressed as

$$\sigma_{y,overall}^* = \frac{W_{tri}}{W}\sigma_{y, tri} + \frac{W_s}{W}\sigma'_s \tag{6}$$

$$\sigma_{y,overall}^* = \frac{W_{tri}}{W} \sigma'_{tri} + \frac{W_s}{W} \sigma_{ys} \quad (7)$$

where σ'_s is the stress in the solid wall portion caused by the strain resulting from the yielding of the lattice structure, i.e., $\sigma'_s = E_s(\sigma_{y,tri}/E_{tri})$, and σ'_{tri} is the stress in the lattice portion caused by the strain resulting from the yielding of the solid wall portion, i.e., $\sigma'_{tri} = E_{tri}(\sigma_{ys}/E_s)$. Since the yield strength of the overall structure depends on which portion reaches the yield point first, Equation (6) is used when the lattice portion reaches the yield point before the wall portion, and vice versa for Equation (7).

2.5. Weight Efficiency

Infill specimens used in this study were designed to reduce their weight by customizing their infill density. Regarding efficiency, the infill specimens with different relative densities cannot be directly compared. Therefore, the ratio between a considered mechanical property per weight density of the specimen and the mechanical property per weight density of a full-solid specimen having the same dimensions was defined as the weight efficiency. The weight efficiency was used to assess the efficiency of an infill specimen compared to its full-solid counterpart, which can be expressed as

$$e_s = \frac{\left(\frac{S^*}{\rho^*}\right)}{\left(\frac{S'}{\rho'}\right)} = \frac{1}{\bar{\rho}} \frac{S^*}{S'} \quad (8)$$

where S^* and S' are mechanical properties considered for the infill specimen and the full-solid counterpart, respectively. The mechanical properties considered for assessing the weight efficiency in this study consist of the elastic modulus and the ultimate tensile strength. In addition, $\bar{\rho}$ denotes the relative density, which is the ratio between the weight density of the infill specimen and the weight density of the full-solid specimen having the same dimensions, i.e., $\bar{\rho} = \rho^*/\rho'$. The average values of the relative density of the specimens in this study are presented in Table 2.

3. Results and Discussion

In this study, a full-solid specimen was considered as a specimen with 100% density equivalent. The stress–strain relations of 316L and 17-4PH stainless steel full-solid specimens obtained from the tensile test are presented in Figure 7. It can be seen that the 17-4PH specimens have more strength than the 316L specimens. The 316L specimens have ductile behavior, while the 17-4PH specimens have brittle behavior.

The average values of the mechanical properties of the 316L and 17-4PH full-solid specimens obtained from the tensile test are shown in Table 3. The yield and ultimate strength of the 17-4PH specimens obviously show more values than the 316L specimens. In contrast, the elastic modulus of both 316L and 17-4PH specimens shows similar values. The average elongation value of the 316L specimens is greater than that of the 17-4PH specimens, i.e., 54.63% and 3.32% elongation, respectively.

Table 3. The mechanical properties of 316L and 17-4PH stainless steel full-solid specimens.

Material	Elastic Modulus ¹ (GPa)	Yield Strength ¹ (MPa)	Ultimate Strength ¹ (MPa)
316L	167.20 (4.00)	159.74 (6.95)	482.31 (14.30)
17-4PH	160.82 (3.45)	653.25 (8.72)	809.89 (16.02)

¹ Standard deviation is depicted in the brackets (SD).

According to a datasheet provided by Desktop Metal, the yield strength and ultimate strength of the 316L specimens are 165 MPa and 494 MPa, respectively. With the same test standard, the yield strength and ultimate strength experimentally obtained in this study are approximately 96.81% and 97.63% of those in the datasheet, respectively. Additionally, the yield strength and ultimate strength of the 17-4PH specimens are 660 MPa and 1042 MPa,

respectively, while the yield strength and ultimate strength experimentally obtained in this study are approximately 98.98% and 77.72% of those in the datasheet, respectively. This discrepancy could have occurred due to various factors in the manufacturing processes. For this reason, an experimental study is vital for assessing the mechanical properties of the AM parts to reflect their actual behavior in different printing contexts.

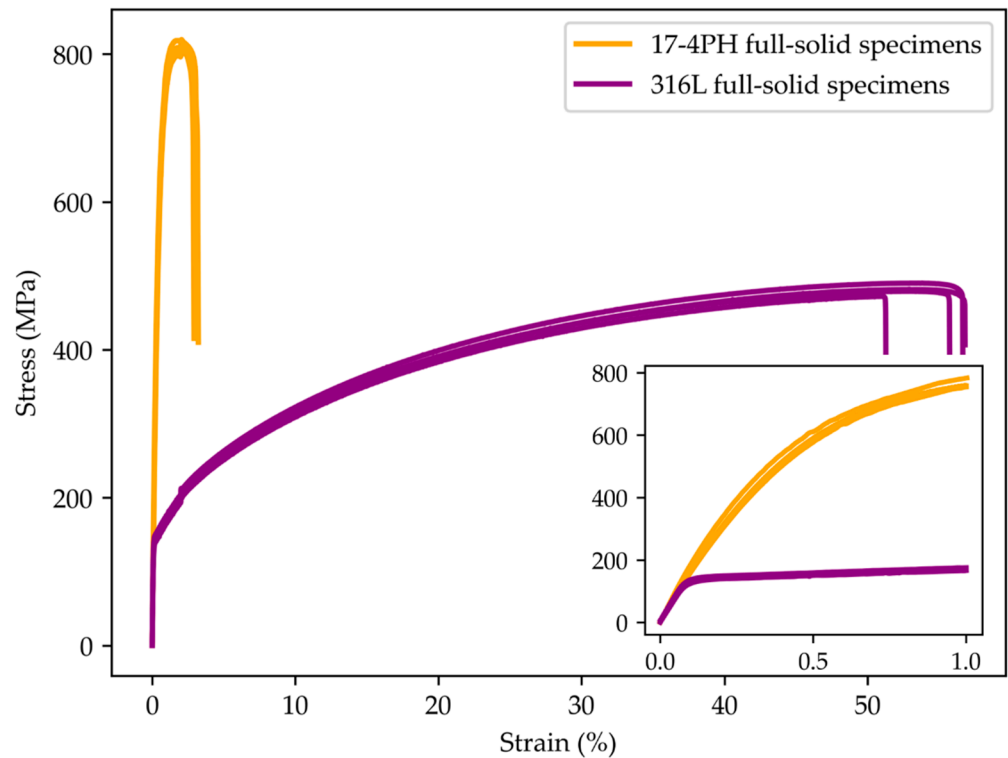


Figure 7. The stress–strain curves of 316L and 17-4PH stainless steel full-solid specimens.

The stress–strain curves of infill specimens made from 316L and 17-4PH stainless steel are shown in Figures 8 and 9, respectively. The 316L infill specimens show lower strength and behave as a ductile material, while the 17-4PH infill specimens show more strength and behave as a brittle material. Note that the shift of the curves at a strain value of 2% in Figure 8 is the effect of the test speed change. Meanwhile, the yield point of the 17-4PH specimens cannot be indicated since the specimens failed near the ultimate strength.

The stress–strain curve comparison of the infill and full-solid specimens made from 316L and 17-4PH stainless steel are illustrated in Figures 10 and 11, respectively, to show the distinctness of material behaviors when the full-solid specimens have their weight reduced using an infill pattern.

Moreover, the mechanical properties of 316L and 17-4PH infill specimens obtained from the tensile test and computed from the analytical method described in Section 2.4 are compared in Table 4. It can be observed that the values of the elastic modulus of the 316L and 17-4PH infill specimens are similar in each relative density.

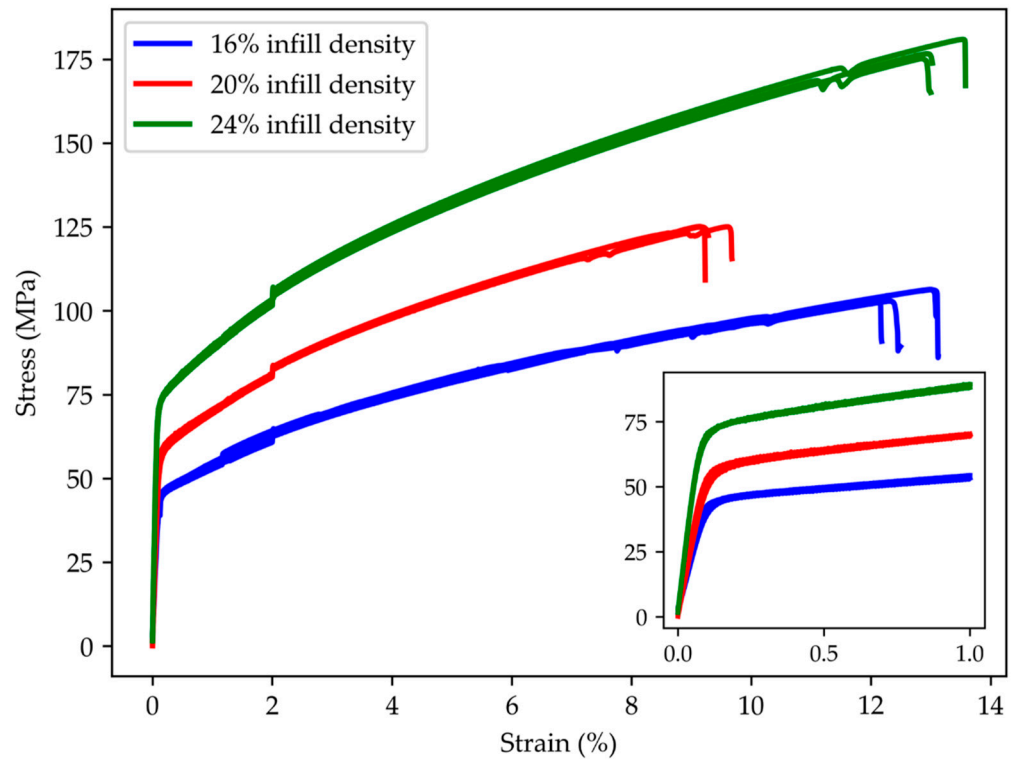


Figure 8. The stress–strain curves of 316L stainless steel infill specimens.

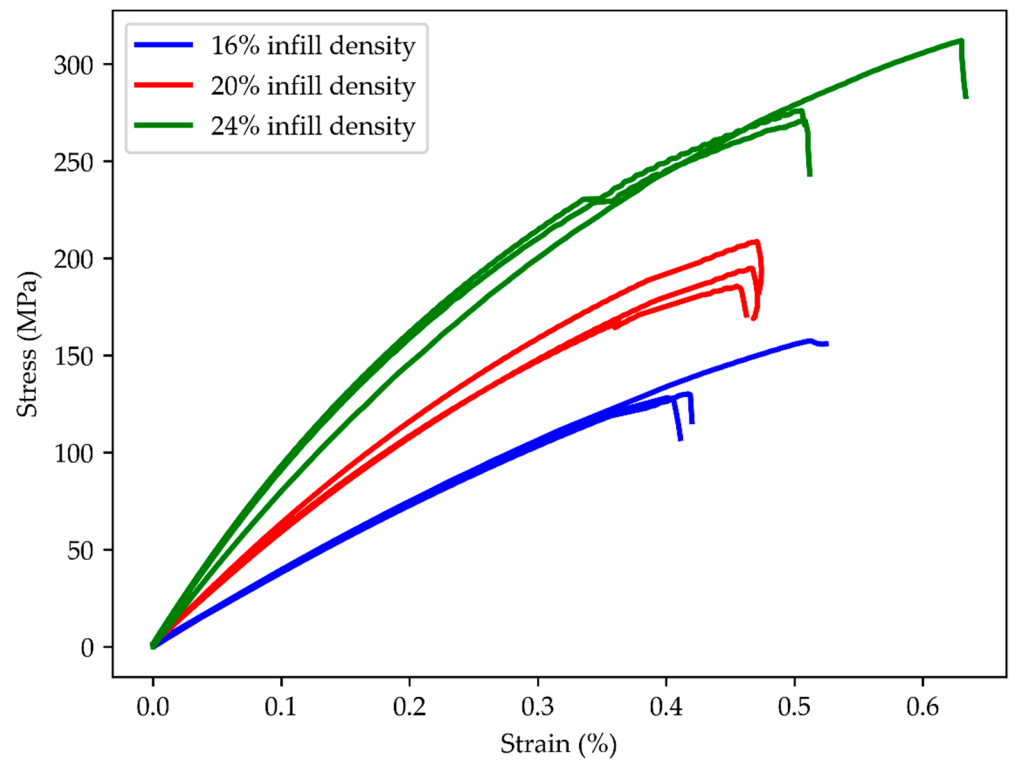


Figure 9. The stress–strain curves of 17-4PH stainless steel infill specimens.

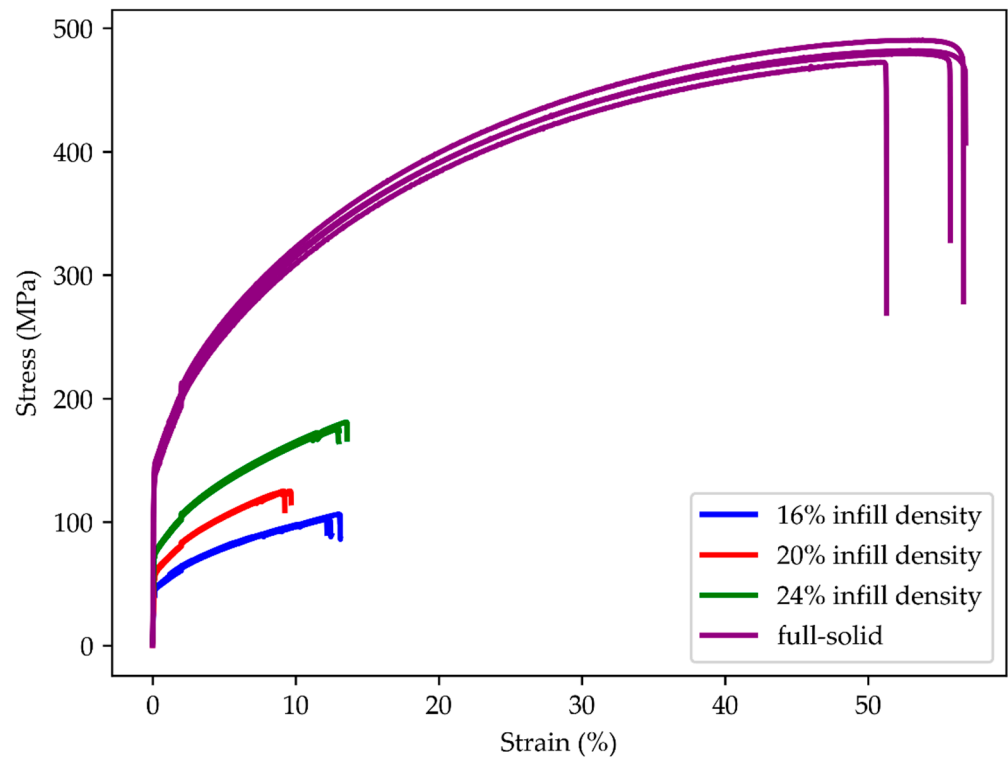


Figure 10. The comparison of stress–strain curves between infill and full-solid specimens made from 316L stainless steel.

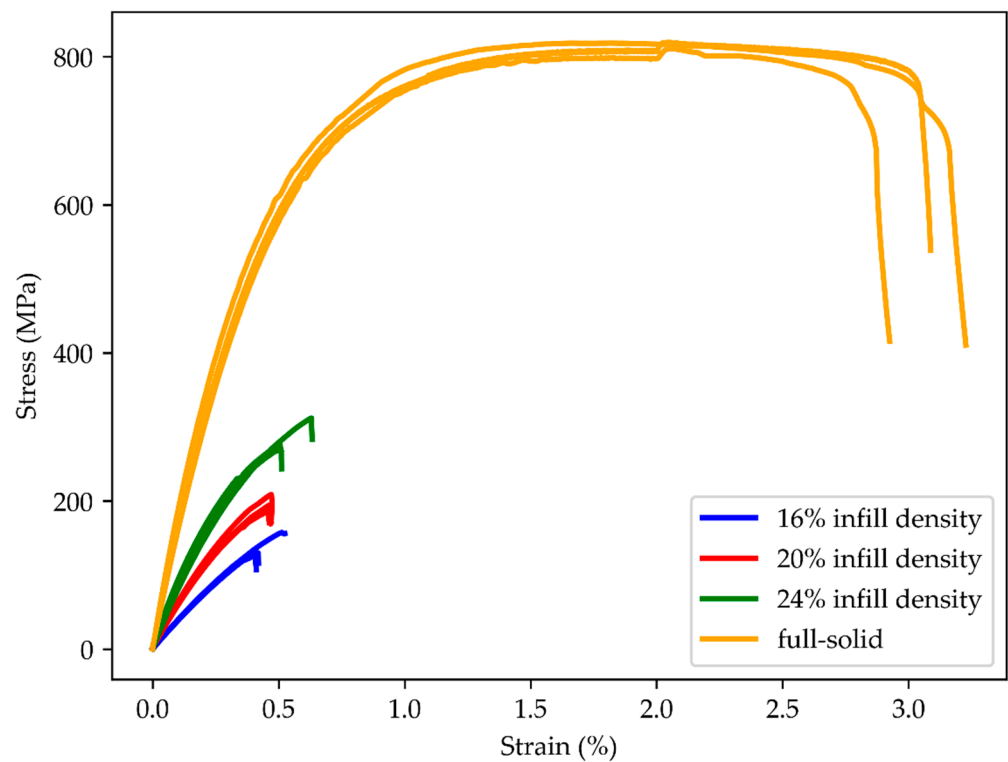


Figure 11. The comparison of stress–strain curves between infill and full-solid specimens made from 17-4PH stainless steel.

Table 4. The mechanical properties of the infill specimens obtained from the tensile tests and analytical methods.

Material	Relative Density (%)	Elastic Modulus ¹ (GPa)			Yield Strength ¹ (MPa)		Ultimate Strength ¹ (MPa)
		Experimental Study	Analytical Method [17]	Analytical Method [19]	Experimental Study	Analytical Method [17]	Experimental Study
316L	50.48	44.18 (1.89)	42.95	43.52	47.31 (0.34)	41.78	100.83 (1.29)
	61.87	54.89 (4.43)	50.34	51.43	63.68 (2.26)	48.98	124.91 (0.28)
	72.94	76.07 (5.60)	57.73	59.59	78.54 (2.57)	56.17	164.02 (3.66)
17-4PH	50.68	42.51 (2.77)	41.31	41.86	-	-	155.05 (3.37)
	62.19	53.28 (2.60)	48.42	49.47	-	-	198.36 (6.60)
	73.60	74.73 (3.18)	55.53	57.32	-	-	271.97 (5.11)

¹ Standard deviation is depicted in the brackets (SD).

With the assumption mentioned in Section 2.4, the analytical method can be used to accurately predict the mechanical properties if the lattice structures have a low relative density. In this study, the elastic modulus of the specimen with a lower relative density (50.48% and 50.68% relative densities) shows a good agreement between the results obtained from the analytical method and the experimental study. The discrepancy between the results obtained from both methods increases for the specimens with a higher relative density.

For the elastic modulus, since some dimensional properties of unit-cell struts are included in the formula of [19], the results obtained from [19] are slightly closer to the experimental results than those obtained from [17]. The yield strength values obtained from the analytical method in the work by [17] are lower than those obtained from the experiment. With the considered relative densities in this study, the wall portion of all infill specimens reaches the yield point before the lattice portion. Thus, Equation (7) was used to compute the yield strength for this case. The discrepancy between the results obtained from Equation (7) and the experiment also increases, caused by the discrepancy in the elastic modulus results. Since, in the rule-of-mixtures model, the yield strength is a function of the elastic modulus, the prediction of the yield strength yields an accurate result for the specimens with a low relative density.

The experimental results of the tensile test show that, when the relative density of the specimens increases, the mechanical properties rapidly increase. For example, when considering the relationship between the elastic modulus and the relative densities, the relation is non-linear for specimens with a higher relative density [23].

The 316L specimens were used in the fatigue test because this material is widely used in many applications with excellent corrosion resistance and ductility. The ultimate tensile strength values of the full-solid and infill specimens in Tables 3 and 4 were used to define the stress level of the specimen for each considered infill density, i.e., 16%, 20%, 24%, and 100% equivalent (full-solid). The geometry and dimensions of the samples in the fatigue test are the same as those in the tensile test. The fatigue results of eight to ten samples were collected for each infill density. The S–N data of the full-solid specimens and infill specimens plotted in both linear–log and log–log scales are shown in Figures 12 and 13, respectively. The stress values between 30% and 90% of the ultimate tensile strength were used to set the maximum stresses for each level in the fatigue test.

It can be observed that the fatigue limits of the specimens with 16% and 20% infill densities show a slight difference, while that of the specimens with 24% infill density shows a considerably higher fatigue limit. It is implied that the relationship between the fatigue behavior and the relative density is also non-linear when the specimens have a higher relative density.

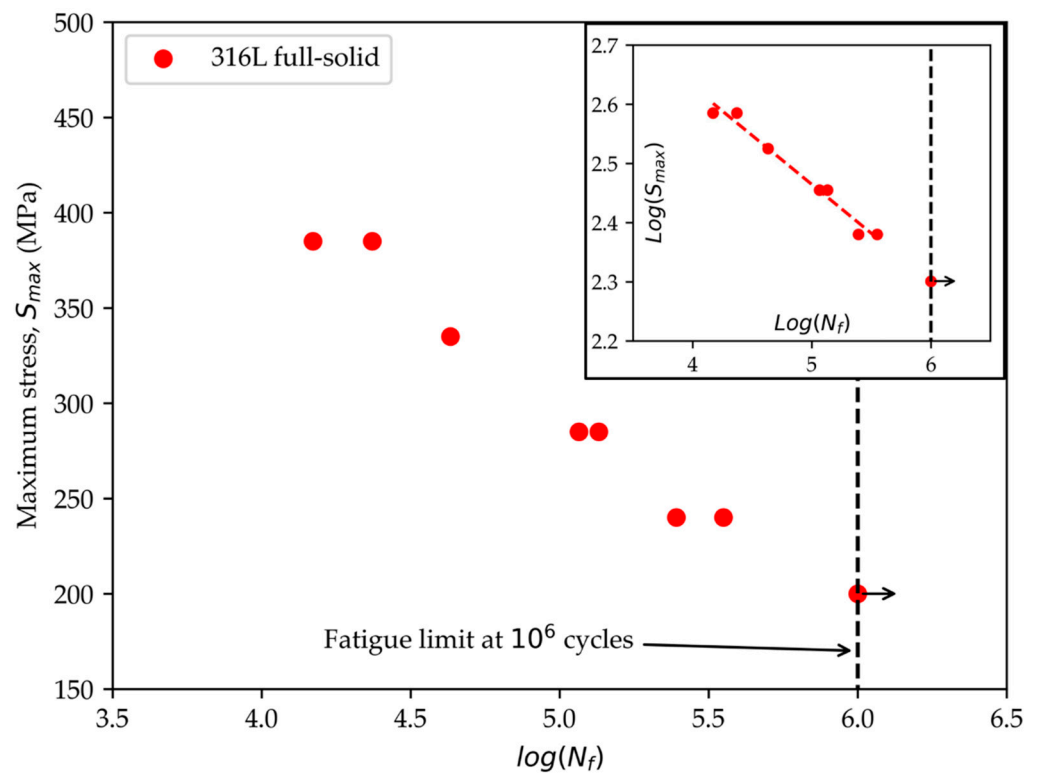


Figure 12. S–N curves of the 316L full-solid specimens in a linear–log plot and linear fitting in a log–log plot.

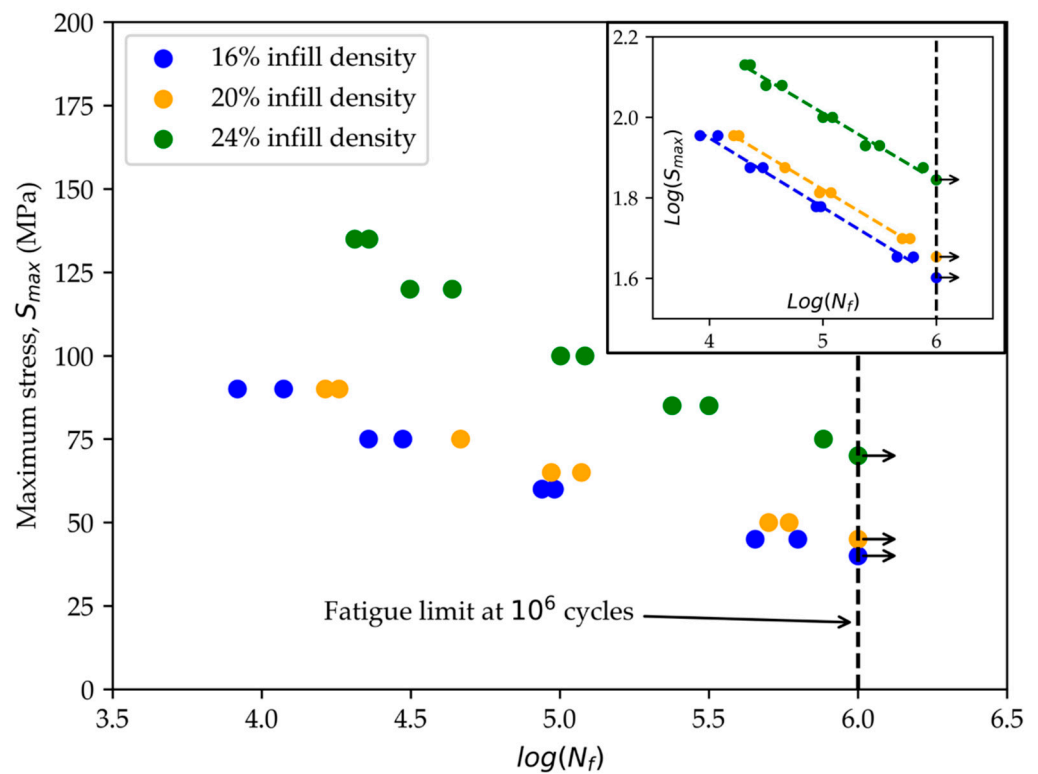


Figure 13. S–N curves of 316L infill specimens with different densities in a linear–log plot and linear fitting in a log–log plot.

To estimate the lifetime of the specimens with different stress levels, a relationship between the maximum stress S_{max} and lifecycle N_f can be expressed as

$$S_{max} = A(N_f)^B \quad (9)$$

where A and B are constant parameters obtained from curve fitting using linear regression, as shown in Figures 12 and 13, in which the relationship between $\log(S_{max})$ and $\log(N_f)$ is linear. The A and B parameters for each relative density of the infill specimens and the fatigue limit at 10^6 cycles are presented in Table 5. In linear regression, the determination (R^2) is used to measure how well the data fit the regression model or the goodness of fit.

Table 5. The constants from linear fittings and fatigue limit of the 316L specimens.

Material	Relative Density (%)	A	B	R^2	Fatigue Limit at 10^6 Cycles (MPa)
316L	50.48	432.91	−0.172	0.990	40
	61.87	464.46	−0.169	0.995	45
	72.94	705.92	−0.168	0.984	70
	100 (equivalent)	1952.29	−0.165	0.975	200

The fatigue test results show a good fitting, with R^2 close to 1. As expected, the specimens with a higher relative density show a greater fatigue limit and A parameters, while B yields similar constant values.

The weight efficiency, defined as the relationship between a considered mechanical property and the relative density, can be computed using Equation (8). The elastic modulus and ultimate tensile strength were the mechanical properties considered for calculating the weight efficiency, i.e., e_E and e_{UTS} . Table 6 shows the values of the weight efficiency with different relative densities.

Table 6. Weight efficiency of 316L and 17-4PH specimens.

Material	Infill Density (%)	Relative Density (%)	Weight Efficiency	
			e_E	e_{UTS}
316L	16	50.48	0.52	0.41
	20	61.87	0.53	0.42
	24	72.94	0.62	0.47
17-4PH	16	50.68	0.52	0.38
	20	62.19	0.53	0.39
	24	73.60	0.63	0.46

The weight efficiency is used to assess the efficiency of the infill specimens with different densities by concerning the mechanical properties and weight of the specimens. In fact, the greater the relative density, the more weight efficiency of the specimens. Nevertheless, this behavior is not linear because the weight efficiency rapidly increases when an infill specimen is denser, closer to being a full-solid one. Thus, selecting an appropriate relative density for the infill specimens could be taken into account to minimize the weight. It can be seen from Table 6 that the values of e_E of the 316L and 17-4PH infill specimens are similar, while the values of e_{UTS} are slightly different. The e_E and e_{UTS} show little difference between the 316L and 17-4PH specimens, with 16% and 20% infill densities. In contrast, the e_E and e_{UTS} of the specimens with 24% infill density show a noticeable increase. It is implied that, if the weight is a major consideration, the specimens with 16% and 20% infill densities yielding similar performance per weight can be used. However, when strength is the main requirement, the specimens with 24% infill density may be a better choice. Note that the reduced weight of the specimens with a lower relative density influences the time and costs in the manufacturing process.

4. Conclusions

This study investigated the mechanical properties of additively manufactured metal materials, including 316L and 17-4PH stainless steel, under static and cyclic loading in tensile mode. The full-solid and infill specimens were fabricated by MAM using the BMD technique. The infill density of 16%, 20%, and 24% was set for the infill specimens, corresponding to a relative density of 50% to 75%, approximately. The full-solid specimen considered to have a 100% relative density equivalent was investigated to obtain the properties of the base materials. The results showed that the 17-4PH full-solid specimens behave as a brittle material and have higher strength than the 316L full-solid specimens. In contrast, the 316L specimens have more elongation and ductility. For the infill specimens, as expected, a higher relative density produces stronger specimens with a higher elastic modulus. However, this behavior is not entirely linear. The relationship between the mechanical properties and the relative density is linear when the specimen has a low relative density and rapidly increases when the relative density approaches a full-solid.

The analytical methods described in Section 2.4 were used to validate the experimental results in this study by comparing the values of an elastic modulus and yield strength of 316L and the values of the elastic modulus of 17-4PH infill specimens. Good agreement is observed between both methods for the specimens with a low relative density, while more discrepancy presents when the relative density increases. Since the formulas were derived using the Euler–Bernoulli beam theory, it cannot be used to predict the mechanical properties of the infill specimens with a high value of the ratio between b and l , namely a high relative density. However, this analytical procedure can be satisfactorily used in the initial evaluation to determine the mechanical properties of the infill specimens with a low relative density.

Regarding the cyclic test, 316L stainless steel was selected for the test specimens because of its ductility and widespread application. The fatigue test was performed with the maximum stress, ranging from 30% to 90% of the ultimate tensile strength of each specimen with different relative densities. The results showed that the fatigue behavior is similar to the tensile strength one; the infill specimens with a higher relative density have a higher fatigue strength for every stress level. The fatigue behavior is also a non-linear function of the relative density, especially when the specimens have a high relative density.

The specimens with 16% and 20% infill densities yield slightly different weight efficiency, while those with 24% infill density show an outstanding weight efficiency. As a result, in terms of weight efficiency, the AM parts with a low relative density cannot compete with those that have a relative density. If lightweight AM parts are required, their relative densities between 50% and 60% of the full-solid counterparts can be considered. In contrast, a high relative density close to the full-solid one is recommended if the strength of AM parts is needed. However, the dense parts affect the time and costs in the manufacturing process. Thus, a specific core design requirement is vital for making a decision.

Author Contributions: Conceptualization, P.S. and T.F.; Methodology, I.T., P.S. and T.F.; Software, I.T. and Y.M.; Validation, I.T. and P.S.; Formal Analysis, I.T. and P.S.; Investigation, I.T. and P.S.; Resources, T.F.; Data Curation, I.T. and Y.M.; Writing—Original Draft Preparation, I.T. and P.S.; Writing—Review and Editing, P.S.; Visualization, I.T. and P.S.; Supervision, T.F.; Project Administration, P.S.; Funding Acquisition, P.S. and T.F. All authors have read and agreed to the published version of the manuscript.

Funding: This work (Grant No. RGNS 64-070) was supported by Office of the Permanent Secretary, Ministry of Higher Education, Science, Research and Innovation (OPS MHESI), Thailand Science Research and Innovation (TSRI) and Chiang Mai University.

Institutional Review Board Statement: Not applicable.

Informed Consent Statement: Not applicable.

Data Availability Statement: Not applicable.

Acknowledgments: This work was partially funded by Chiang Mai University, Thailand. The first author received the TA/RA scholarship from the Graduate School, Chiang Mai University, and the scholarship from the Faculty of Engineering, Chiang Mai University.

Conflicts of Interest: The authors declare no conflict of interest.

References

1. Abduo, J.; Lyons, K.; Bennamoun, M. Trends in computer-aided manufacturing in prosthodontics: A review of the available streams. *Int. J. Dent.* **2014**, *2014*, 783948. [[CrossRef](#)] [[PubMed](#)]
2. Jandyal, A.; Chaturvedi, I.; Wazir, I.; Raina, A.; Ul Haq, M.I. 3D printing—A review of processes, materials and applications in industry 4.0. *Sustain. Oper. Comput.* **2022**, *3*, 33–42. [[CrossRef](#)]
3. Subeshan, B.; Baddam, Y.; Asmatulu, E. Current progress of 4D-printing technology. *Prog. Addit. Manuf.* **2021**, *6*, 495–516. [[CrossRef](#)]
4. Jia, D.; Li, F.; Zhang, Y. 3D-printing process design of lattice compressor impeller based on residual stress and deformation. *Sci. Rep.* **2020**, *10*, 600. [[CrossRef](#)] [[PubMed](#)]
5. Vasques, C.M.A.; Gonçalves, F.C.; Cavadas, A.M.S. Manufacturing and Testing of 3D-Printed Polymer Isogrid Lattice Cylindrical Shell Structures. In Proceedings of the 2nd International Electronic Conference on Applied Sciences, Online, 15–21 October 2021.
6. Blakey-Milner, B.; Gradl, P.; Snedden, G.; Brooks, M.; Pitot, J.; Lopez, E.; Leary, M.; Berto, F.; du Plessis, A. Metal additive manufacturing in aerospace: A review. *Mater. Des.* **2021**, *209*, 110008. [[CrossRef](#)]
7. Khorasani, M.; Ghasemi, A.; Rolfe, B.; Gibson, I. Additive manufacturing a powerful tool for the aerospace industry. *Rapid Prototyp. J.* **2021**, *28*, 1355–2546. [[CrossRef](#)]
8. Adamczak, S.; Bochnia, J.; Kaczmarska, B. An Analysis of Tensile Test Results to Assess the Innovation Risk for an Additive Manufacturing Technology. *Metrol. Meas. Syst.* **2015**, *22*, 127–138. [[CrossRef](#)]
9. Hsueh, M.H.; Lai, C.J.; Liu, K.Y.; Chung, C.F.; Wang, S.H.; Pan, C.Y.; Huang, W.C.; Hsieh, C.H.; Zeng, Y.S. Effects of Printing Temperature and Filling Percentage on the Mechanical Behavior of Fused Deposition Molding Technology Components for 3D Printing. *Polymers* **2021**, *13*, 2910. [[CrossRef](#)]
10. Johnson, G.A.; French, J.J. Evaluation of infill effect on mechanical properties of consumer 3D printing materials. *Adv. Technol. Innov.* **2018**, *3*, 179.
11. Khan, S.A.; Siddiqui, B.A.; Fahad, M.; Khan, M.A. Evaluation of the Effect of Infill Pattern on Mechanical Strength of Additively Manufactured Specimen. *Mater. Sci. Forum* **2017**, *887*, 128–132. [[CrossRef](#)]
12. Letcher, T.; Rankouhi, B.; Javadpour, S. Experimental Study of Mechanical Properties of Additively Manufactured ABS Plastic as a Function of Layer Parameters. In Proceedings of the ASME 2015 International Mechanical Engineering Congress and Exposition, Houston, TX, USA, 13–19 November 2019.
13. Caminero, M.Á.; Gutiérrez, A.R.; Chacón, J.M.; García-Plaza, E.; Núñez, P.J. Effects of fused filament fabrication parameters on the manufacturing of 316L stainless-steel components: Geometric and mechanical properties. *Rapid Prototyp. J.* **2022**, *ahead-of-print*. [[CrossRef](#)]
14. Suwanprecha, C.; Manonukul, A. On the build orientation effect in as-printed and as-sintered bending properties of 17-4PH alloy fabricated by metal fused filament fabrication. *Rapid Prototyp. J.* **2022**, *28*, 1355–2546. [[CrossRef](#)]
15. Gasparetto, V.; ElSayed, M. Multiscale Modelling and Mechanical Anisotropy of Periodic Cellular Solids with Rigid-Jointed Truss-Like Microscopic Architecture. *Appl. Mech.* **2021**, *2*, 331–355. [[CrossRef](#)]
16. Gu, H.; Pavier, M.; Shterenlikht, A. Experimental study of modulus, strength and toughness of 2D triangular lattices. *Int. J. Solids Struct.* **2018**, *152–153*, 207–216. [[CrossRef](#)]
17. Wang, A.J.; McDowell, D.L. In-Plane Stiffness and Yield Strength of Periodic Metal Honeycombs. *J. Eng. Mater. Technol.* **2004**, *126*, 137–156. [[CrossRef](#)]
18. Theerakittayakorn, K.; Suttakul, P.; Sam, P.; Nanakorn, P. Design of frame-like periodic solids for isotropic symmetry by member sizing. *J. Mech.* **2017**, *33*, 41–54. [[CrossRef](#)]
19. Sam, P.; Nanakorn, P.; Theerakittayakorn, K.; Suttakul, P. Closed-form effective elastic constants of frame-like periodic cellular solids by a symbolic object-oriented finite element program. *Int. J. Mech. Mater. Des.* **2016**, *13*, 363–383. [[CrossRef](#)]
20. Somnic, J.; Jo, B.W. Status and Challenges in Homogenization Methods for Lattice Materials. *Materials* **2022**, *15*, 605. [[CrossRef](#)]
21. Wu, Y.; Yang, L. The effect of unit cell size and topology on tensile failure behavior of 2D lattice structures. *Int. J. Mech. Sci.* **2020**, *170*, 105342. [[CrossRef](#)]
22. Suttakul, P.; Fongsamootr, T.; Vo, D.; Nanakorn, P. Effects of Shear Deformation of Struts in Hexagonal Lattices on their Effective In-Plane Material Properties. *Mater. Sci. Forum* **2021**, *1034*, 193–198. [[CrossRef](#)]
23. Yazdanparast, R.; Rafiee, R. Determining in-plane material properties of square core cellular materials using computational homogenization technique. *Eng. Comput.* **2022**. [[CrossRef](#)]
24. Limpitipanich, P.; Suttakul, P.; Mona, Y.; Fongsamootr, T. Material Behavior of 2D Steel Lattices with Different Unit-Cell Patterns. *Mater. Sci. Forum* **2021**, *1046*, 15–21. [[CrossRef](#)]
25. Fongsamootr, T.; Suttakul, P.; Tippayawong, N.; Nanakorn, P.; Cappellini, C. Bending Behavior of 2D Periodic Plates With Different Unit Cells: Numerical and Experimental Investigations. *Mater. Today Commun.* **2022**, *31*, 103774. [[CrossRef](#)]

26. Bjørheim, F.; Lopez, I.L.T. Tension testing of additively manufactured specimens of 17-4 PH processed by Bound Metal Deposition. In Proceedings of the IOP Conference Series: Materials Science and Engineering, Moscow, Russia, 25–26 November 2021.
27. Gabilondo, M.; Cearsolo, X.; Arrue, M.; Castro, F. Influence of Build Orientation, Chamber Temperature and Infill Pattern on Mechanical Properties of 316L Parts Manufactured by Bound Metal Deposition. *Materials* **2022**, *15*, 1183. [[CrossRef](#)]
28. Iacopo, B.; Tommaso, M.; Massimiliano, P.; Alessio, V. Environmental impacts assessment of Bound Metal Deposition 3D printing process for stainless steel. *Procedia CIRP* **2022**, *105*, 386–391. [[CrossRef](#)]
29. Gao, C.; Wolff, S.; Wang, S. Eco-friendly additive manufacturing of metals: Energy efficiency and life cycle analysis. *J. Manuf. Syst.* **2021**, *60*, 459–472. [[CrossRef](#)]
30. Porro, M.; Zhang, B.; Parmar, A.; Shin, Y.C. Data-Driven Modeling of Mechanical Properties for 17-4 PH Stainless Steel Built by Additive Manufacturing. *Integr. Mater. Manuf. Innov.* **2022**, *11*, 241–255. [[CrossRef](#)]
31. Sezer, H.; Tang, J.; Ahsan, A.N.; Kaul, S. Modeling residual thermal stresses in layer-by-layer formation of direct metal laser sintering process for different scanning patterns for 316L stainless steel. *Rapid Prototyp. J.* **2022**, *ahead-of-print*. [[CrossRef](#)]
32. Chen, W.; Spätig, P.; Seifert, H.P. Role of mean stress on fatigue behavior of a 316L austenitic stainless steel in LWR and air environments. *Int. J. Fatigue* **2021**, *145*, 106111. [[CrossRef](#)]
33. Mohammad, K.A.; Zainudin, E.S.; Sapuan, S.M.; Zahari, N.I.; Aidi, A. Fatigue Life for Type 316L Stainless Steel under Cyclic Loading. *Adv. Mater. Res.* **2013**, *701*, 77–81. [[CrossRef](#)]
34. Ueno, H.; Kakihata, K.; Kaneko, Y.; Hashimoto, S.; Vinogradov, A. Enhanced fatigue properties of nanostructured austenitic SUS 316L stainless steel. *Acta Mater.* **2011**, *59*, 7060–7069. [[CrossRef](#)]
35. Mower, T.M.; Long, M.J. Mechanical behavior of additive manufactured, powder-bed laser-fused materials. *Mater. Sci. Eng. A* **2016**, *651*, 198–213. [[CrossRef](#)]
36. Spierings, A.B.; Starr, T.L.; Wegener, K. Fatigue performance of additive manufactured metallic parts. *Rapid Prototyp. J.* **2013**, *19*, 88–94. [[CrossRef](#)]
37. Werner, T.; Madia, M.; Zerbst, U. Comparison of the fatigue behavior of wrought and additively manufactured AISI 316L. *Procedia Struct. Integr.* **2022**, *38*, 554–563. [[CrossRef](#)]
38. Ardi, D.T.; Guowei, L.; Maharjan, N.; Mutiargo, B.; Leng, S.H.; Srinivasan, R. Effects of post-processing route on fatigue performance of laser powder bed fusion Inconel 718. *Addit. Manuf.* **2020**, *36*, 101442. [[CrossRef](#)]
39. Brodie, E.G.; Richter, J.; Wegener, T.; Molotnikov, A.; Niendorf, T. Influence of a remelt scan strategy on the microstructure and fatigue behaviour of additively manufactured biomedical Ti65Ta efficiently assessed using small scale specimens. *Int. J. Fatigue* **2022**, *162*, 106944. [[CrossRef](#)]
40. Gribbin, S.; Bicknell, J.; Jorgensen, L.; Tsukrov, I.; Knezevic, M. Low cycle fatigue behavior of direct metal laser sintered Inconel alloy 718. *Int. J. Fatigue* **2016**, *93*, 156–167. [[CrossRef](#)]
41. Maskery, I.; Aboulkhair, N.; Tuck, C.; Wildman, R.; Ashcroft, I.; Everitt, N.; Hague, R. Fatigue Performance Enhancement of Selectively Laser Melted Aluminum Alloy by Heat Treatment. In Proceedings of the 2015 International Solid Freeform Fabrication Symposium, Austin, TX, USA, 10–12 August 2015.
42. Solberg, K.; Torgersen, J.; Berto, F. Fatigue Behaviour of Additively Manufactured Inconel 718 Produced by Selective Laser Melting. *Procedia Struct. Integr.* **2018**, *13*, 1762–1767. [[CrossRef](#)]
43. *ASTM E8/E8M-16a*; Standard Test Methods for Tension Testing of Metallic Materials. ASTM International: West Conshohocken, PA, USA, 2016.
44. *ASTM E466*; Standard Practice for Conduction Force Controlled Constant Amplitude Axial Fatigue Test of Metallic Materials. Annual Book of ASTM Standards. ASTM International: West Conshohocken, PA, USA, 2002.
45. Suttakul, P.; Nanakorn, P.; Vo, D. Effective out-of-plane rigidities of 2D lattices with different unit cell topologies. *Arch. Appl. Mech.* **2019**, *89*, 1837–1860. [[CrossRef](#)]
46. Suttakul, P.; Chaichanasiri, E.; Nanakorn, P. Design of 2D-Lattice Plates by Weight Efficiency. *Eng. J.* **2021**, *25*, 13–31. [[CrossRef](#)]
47. Hyer, M.W.; White, S.R. *Stress Analysis of Fiber-Reinforced Composite Materials*; DEStech Publications, Inc.: Lancaster, PA, USA, 2009.